# Surface-Enhanced Raman Spectroelectrochemical Studies of Corrosion Films on Iron in Aqueous Carbonate Solution

**L. J. Simpson**[*,a] **and C. A. Melendres**[a,b,*]

[a]*Chemical Technology Division and* [b]*Materials Science Division, Argonne National Laboratory, Argonne, Illinois 60439, USA*

ABSTRACT

The corrosion films on iron in aqueous carbonate/bicarbonate solutions were studied as a function of concentration, pH, and temperature by using the technique of surface-enhanced Raman spectroscopy with electrodeposited silver. Both $Fe(OH)_2$ and $Fe_3O_4$ were detected in the surface oxide film at prepassivation potentials. Iron carbonate (siderite) was observed in the corrosion film in a limited pH, temperature, and applied potential range. At lower carbonate/bicarbonate concentration (*e.g.*, 0.01 *M*), passivation was lost, and continuous anodic dissolution of the iron occurred. The cathodic reduction of the corrosion film was enhanced at 75°C.

## Introduction

The corrosion of iron and mild steel is a fundamental academic and industrial concern that has received a considerable amount of attention.[1-9] Open-air and aerated water systems are among the most common environments in which the corrosion of iron occurs.[2] Corrosion inhibition is most easily accomplished by directing the formation of corrosion products that promote a self-inhibition of the corrosion processes.[3] To achieve this, a complete understanding of the corrosion process and the structure of the passive film is required for the system of interest. Specifically, we are interested in cooling water systems that are open to the atmosphere and contain ambient equilibrium concentrations of oxygen and carbon dioxide.[4-6]

Surface layer formation requires corrosion products with very low solubilities.[3] Complete metal protection (and thus corrosion inhibition) is achieved when iron oxides, hydroxides, and other compounds physically separate the metal from the solution.[4] In general, porosity, surface structure, and composition must be considered in determining the optimum protective layer, but no layer is perfect. We consider only the fundamentals of this protective layer here. In oxygenated water, trivalent iron hydroxide and oxyhydrates have a much lower solubility than divalent iron species and are required in stable corrosion film formation.[4]

A complete understanding of the protective film under cooling water conditions requires investigations at relatively low carbonate/bicarbonate concentrations and at elevated temperatures.[4] Most investigations to date have not used concentrations sufficiently low[10,11] to provide meaningful results, and very few studies have been done at elevated temperatures.[11,12] We investigated the corrosion film on iron, using Raman spectroscopy and electrochemistry, under conditions more appropriate for iron in natural waters containing carbonate and bicarbonate. These measurements were done in 0.002 to 0.05 *M* $Na_2CO_3$ and 0.01 to 0.75 *M* $NaHCO_3$ solutions, at temperatures of 25, 50, and 75°C. The ratio between the carbonate and bicarbonate was varied to provide solution pH of 8.5, 8.7, 9.5, and 11.5. These pH values are representative of the entire pH range permitted by the carbonate/bicarbonate system in aqueous conditions. A solution containing only sodium bicarbonate would have a pH of approximately 8.5, while a solution containing only sodium carbonate would have a pH of approximately 11.5. We provide experimental results as a function of pH, solution concentration, and solution temperature.

## Experimental

Electrochemical control of the iron electrode was provided by an EG&G Princeton Applied Research (EG&G PAR) Model 173 potentiostat, driven by a PAR 179 universal programmer. A saturated calomel electrode (SCE) and a wound platinum wire, with a large surface area (35 $cm^2$) in contact with the solution, were used as the reference and counterelectrode, respectively. All electrochemical potentials presented in this paper refer to the SCE. The electrolyte was made from reverse osmosis purified water with analytical reagent-grade chemicals. A Spex Model 1403 double monochromator, in conjunction with a photomultiplier tube detector and a Spex SCAMP data acquisition controller, were used to obtain the Raman spectra. A Coherent Model Innova 300 $Ar^+$ laser provided the 100 mW of 514.5 nm coherent light used for sample excitation.

A 99.99% pure iron electrode with a surface area of 4 $cm^2$ (0.005 cm thick) was mechanically polished with 600 grit emery paper, degreased with acetone, and thoroughly rinsed with high-purity water. The iron electrode was then held in the electrolyte at a reducing potential of −1.4 V for 30 min. For the surface-enhanced Raman spectroscopy (SERS), after rinsing the carbonate solution off with water, 50 mC/$cm^2$ of Ag was deposited onto the iron surface, at −0.6 V in a 1 m*M* $HNO_3$ + 1 m*M* $AgNO_3$ solution. The iron electrode was again rinsed with water before being placed into the electrochemical cell for the Raman measurements. Immediately upon immersion in the electrochemical cell, the iron electrode was scanned from the −0.3 V open-circuit potential to −1.4 V at 5 mV/s. The iron electrode was held at −1.4 for 5 to 15 min to reduce any air-formed surface film. Subsequent electrochemical procedures used a potential scan rate of 5 mV/s. A Raman spectrum was collected in approximately 1 h by holding the iron electrode at a specific potential. Changing the potential with the 5 mV/s scan rate allowed for a smooth transition of the corrosion film on the iron that most closely matched the electrochemical cyclic voltammograms (CVs) to which the Raman data were compared and referenced. The time required to transition between the potentials used for the Raman data was minor compared with the time used to allow the system to come to equilibrium and the time required to obtain the Raman spectrum.

## Results and Discussion

For potentials above −0.7 V, the CVs were dominated by the continuous anodic dissolution of the iron at 50°C in 0.01 *M* $NaHCO_3$ solutions for pH between 8.5 and 9.5, and sometimes at the higher concentration of 0.05 *M* $NaHCO_3$ at 75°C. This continuous anodic dissolution greatly impedes any effort to obtain information about the corrosion film on iron in equilibrium with the solution. Figure 1 shows the CV of iron in aerated carbonate/bicarbonate solutions at concentrations between 0.002 to 0.05 *M* $Na_2CO_3$ and 0.01 to 0.75 *M* $NaHCO_3$, at 25°C. In general, up to three anodic oxidation waves are observed, while two reduction waves are evident in the reverse cathodic scans. The waves become more prominent and the peak potentials of the waves shift slightly as the solution concentration is increased. However, concentrations of carbonate or

* Electrochemical Society Active Member.

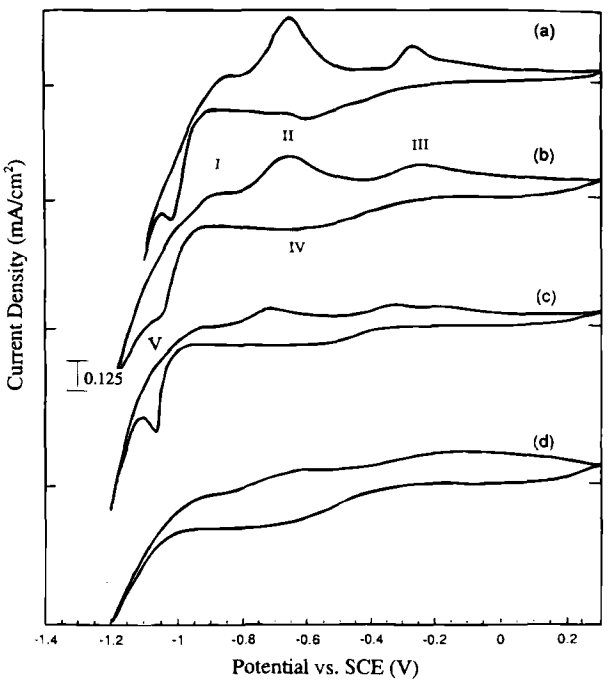


**Fig. 1. CVs of iron in aerated carbonate/bicarbonate electrolytic solutions (pH 9.5): (a) 0.75 *M* $NaHCO_3$ + 0.15 *M* $Na_2CO_3$; (b) 0.25 *M* $NaHCO_3$ + 0.05 *M* $Na_2CO_3$; (c) 0.05 *M* $NaHCO_3$ + 0.01 *M* $Na_2CO_3$; and (d) 0.01 *M* $NaHCO_3$ + 0.002 *M* $Na_2CO_3$.**

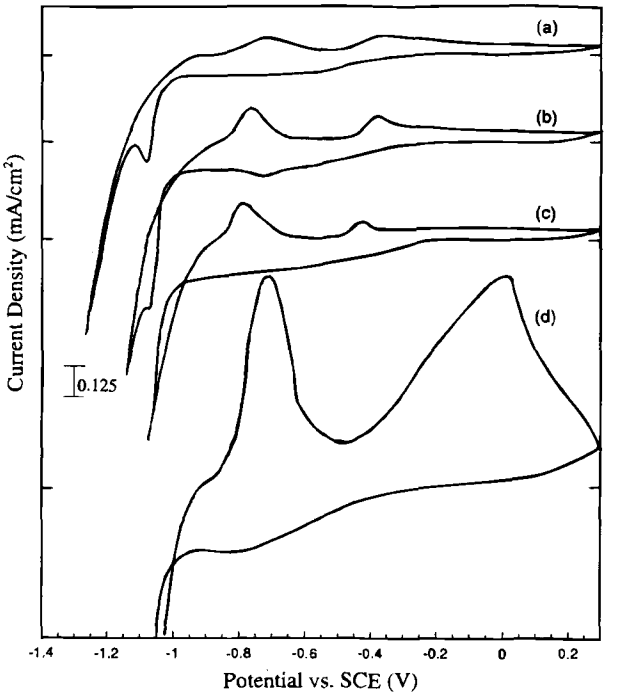


**Fig. 2. CVs of iron in aerated 0.05 *M* $NaHCO_3$ + 0.01 *M* $Na_2CO_3$ solutions (pH 9.5) at 25 (a), 50 (b), and 75°C (c). (d) CV of iron in aerated 0.05 *M* $NaHCO_3$ + 0.001 *M* $Na_2CO_3$ solutions at pH 8.7 and 75°C.**

bicarbonate above approximately 0.05 *M* caused Raman scattering from the solution.[11] The continuous anodic dissolution at higher temperatures and the potential interference of Raman scattering from solution species dictated that we use solution concentrations of approximately 0.05 *M* for the Raman experiments. Figure 2a-c shows the CV of iron in aerated 0.05 *M* $NaHCO_3$ + 0.01 *M* $Na_2CO_3$ solutions at different temperatures (pH 9.5). At 25°C, the voltammograms indicate that the iron electrode forms prepassive film at potentials below approximately −0.7 V and a passive film at higher potentials (Fig. 1 and 2). The voltammograms at 8.7, 9.5, and 11.5 pH are similar in the prepassivation region, even at 25°C where $FeCO_3$ (siderite) forms at pH < 9.5. In fact, little difference could be observed between the pH 9.5 and the pH 11.5 CV at all temperatures and potentials. The notable difference is observed in the enhanced anodic waves in the passivation region of the pH 8.7, 75°C CV (Fig. 2d). This enhancement is ascribed to increased formation of trivalent iron species.[12] A corresponding enhancement in the Raman spectra was not observed. This may be due to an increased formation of a corrosion species not readily observed by Raman, such as FeOOH, or an increase in the amount of soluble species going in solution. The anodic waves also become more prominent and the potentials shift slightly as the temperature is increased.

The need to study the corrosion film on iron *in situ* in an aerated solution significantly enhances the difficulty of maintaining adequate surface control and interpretation of the data. The requirement that the solutions be open to the atmosphere provides a source for airborne contaminants, including $CO_2$ and hydrocarbons.[12,14] The actual corrosion film that provides the passive corrosion inhibition is only a few nanometers thick.[15-18] For most iron species, this thin film does not provide sufficient material for Raman scattering.[10,11,17,18] Recently, surface enhancement of the Raman scattering has been achieved with the aid of silver and gold.[10,17-28] This surface enhancement is sufficient to provide detailed information about the thin passive film on iron. Numerous studies of the silver in similar solutions[13,14] and in carbonate/bicarbonate solutions[24-27] have concluded that silver provides a relatively benign enhancement mechanism. McQuillan *et al.*[24] observed a relatively weak carbonate interaction with a silver electrode in a 0.1 *M* $Na_2CO_3$ solution and even weaker interactions in a bicarbonate solution. The largest effects were observed for the bands at 1540 and 1390 $cm^{-1}$, which were later identified by Cooney and co-workers as $CO_2$ and hydrocarbon bands.[13,14] Sasaki *et al.*[25] provide a complete potential-dependent set of data for a silver electrode in a 0.5 *M* $Na_2CO_3$ solution. The additional solution concentration provided larger Raman signals from the carbonate and thus an enhanced signal-to-noise level for the spectra that allowed the authors to observe most of the known vibrational modes associated with carbonate.[29] These authors also provided Raman spectra at potentials where silver oxides form (above 0.2 V). Thus they were able to identify Raman peaks from silver oxides. It should be noted that any interaction of the Ag with the carbonate was associated with the strong carbonate stretching mode at 1070 $cm^{-1}$. Therefore, any interaction of the silver or the iron with carbonate or bicarbonate should contain this peak. The lack of this peak in a spectrum would indicate that interactions with the carbonate/bicarbonate at the interface is limited. Due to the high solution concentrations used in these previous studies, it is not clear whether the data were effected by the carbonate species in solution. Furthermore, while assignment of a chemisorbed carbonate species was made, no new peaks associated with the Ag-$OCO_2$ bonding were reported.[29] With the relatively low concentrations used in our present investigations, we did not observe any significant carbonate/bicarbonate interactions with the silver from the Raman spectra and would expect to find potential-dependent behavior similar to that reported by Oblonsky and Devine[18] for a silver electrode in borate solution and Cooney *et al.*[14] for a silver electrode in KCl solution.

Electrodeposited silver on iron does not significantly alter interactions between the iron and the electrolytic solution.[10,17-23] The silver does not oxidize under the conditions used in these experiments[13,14,25] but does enhance the detection of trace amounts of carbon (less than 0.1 monolayer) on the electrode surface. Also, the corrosion films on iron have been shown to form homogeneously over the entire surface.[11,30] Therefore, we would expect the corrosion films that we observe with the surface enhancement

effects next to the silver to be representative of the entire corrosion film on the iron electrode. Furthermore, Raman spectra were obtained under conditions where the monitored electrochemistry indicated stable corrosion film development such that continuous dissolution was not occurring.

The SERS effect of carbon, $CO_2$, or hydrocarbons with silver is a fairly well understood process.[13,14,17,18] Amorphous carbon accounts for Raman peaks at 1350 and 1580 $cm^{-1}$, while $CO_2$ accounts for peaks at 1274 and 1383 $cm^{-1}$.[13,14,17,18] The broad peak between 800 and 900 $cm^{-1}$ and the peak at 1444 $cm^{-1}$ are attributed to the C-H vibrational bending modes of hydrocarbon contamination.[13,14,17,18] The effects of most of these contaminants decrease at higher potentials and are more pronounced when other Raman contributions are relatively small. The Raman signals from these contaminants and that of water (1640 $cm^{-1}$)[31] at the iron surface are present throughout most of the Raman data we analyze here. However, unless they have a specific effect on the results of the corrosion film analysis, we do not discuss them further.

Figures 3 to 9 show the potential-dependent Raman spectra between 200 and 1700 $cm^{-1}$ of the iron surface at 25, 50, and 75°C with solution pH of 8.7, 9.5, and 11.5. The individual Raman spectrum in each figure was taken at potentials related to the anodic oxidation and cathodic reduction waves in the voltammograms. The Raman spectra in Fig. 3 to 9a correspond to the "clean" iron surface. These spectra are characterized by a lack of any significant Raman peaks below 800 $cm^{-1}$, indicating a complete or nearly complete reduction of any air-formed oxide on the iron surface. Moving sequentially up the figures, the spectra were taken at potentials just positive of the three anodic oxidation waves. The Raman peak at 544 $cm^{-1}$, after the first anodic wave (Fig. 3 to 9b), corresponds to the presence of $Fe(OH)_2$.[10] Only $Fe(OH)_2$ is detected on the iron surface for pH 9.5 or lower at 25°C. However, for higher temperatures and higher pH, a Raman peak at 664 $cm^{-1}$ is also observed, indicating the presence of $Fe_3O_4$.[18,21] After the second anodic wave, the $Fe(OH)_2$ and $Fe_3O_4$ Raman peak intensities increase (Fig. 3 to 8c), except in Fig. 6c at 25°C, where the siderite bands at 516 and 1070 $cm^{-1}$ dominate the spectrum, and in Fig. 9c, where the peaks lose intensity. At pH 11.5 the Raman peaks attain their maximum intensities (Fig. 9) after the first anodic wave and diminish to almost nothing at 0 V. Weak Raman peaks are observed in the cathodic Raman scans as well, indicating the formation of a passive corrosion film that is not readily identified by Raman spectroscopy. We discuss this in more detail later.

For pH 9.5, the 664 $cm^{-1}$ peak has a maximum intensity after the third anodic wave but remains small relative to the 544 $cm^{-1}$ peak (Fig. 3 to 5d). Both peaks broaden, and

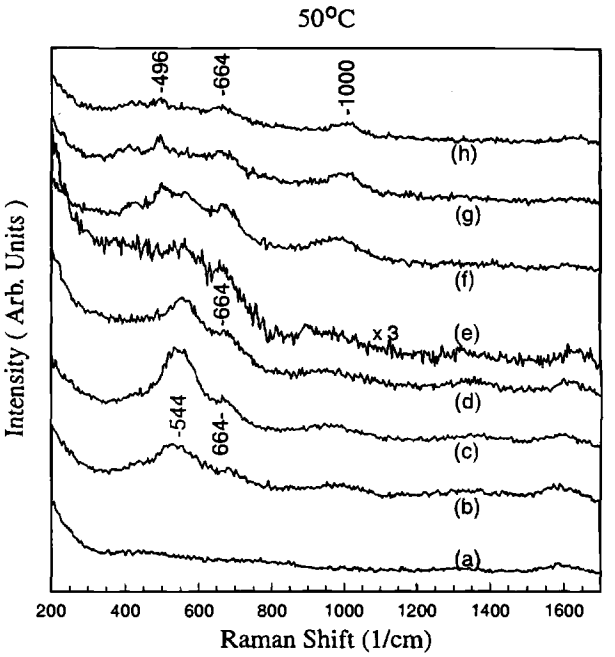


**Fig. 4. SERS of iron in aerated 0.05 *M* $NaHCO_3$ + 0.01 *M* $Na_2CO_3$ solutions (pH 9.5) at 50°C and different potentials: (a) −1.0 V, (b) −0.9 V, (c) −0.6 V, (d) −0.4 V, (e) 0.0 V, (f) −0.7 V, (g) −1.0 V, and (h) −1.2 V. Curves a-e correspond to the anodic sweep, f-h to the cathodic sweep.**

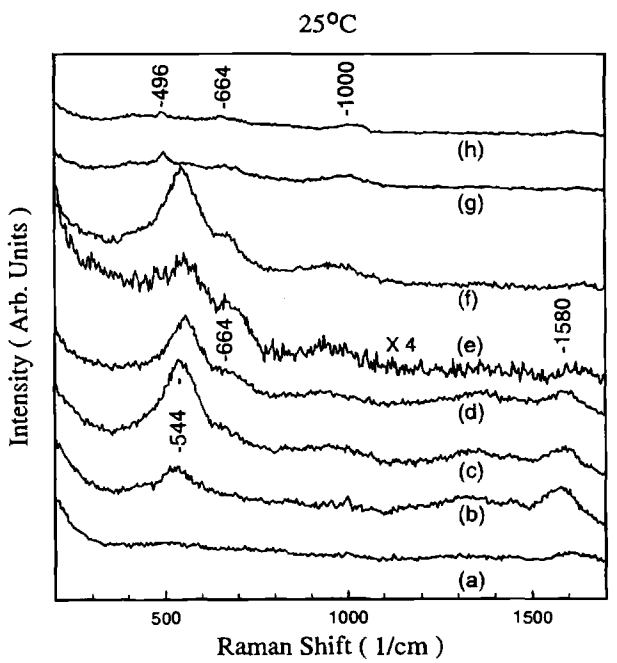


**Fig. 3. SERS of iron in aerated 0.05 *M* $NaHCO_3$ + 0.01 *M* $Na_2CO_3$ solutions (pH 9.5) at 25°C and different potentials: (a) −1.0 V, (b) −0.9 V, (c) −0.6 V, (d) −0.4 V, (e) 0.0 V, (f) −0.7 V, (g) −1.0 V, and (h) −1.2 V. Curves a-e correspond to the anodic sweep, f-h to the cathodic sweep.**

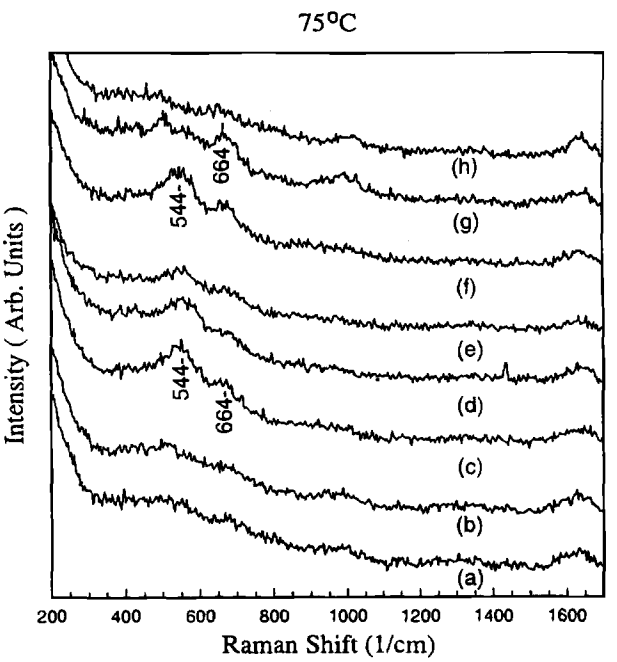


**Fig. 5. SERS of iron in aerated 0.05 *M* $NaHCO_3$ + 0.01 *M* $Na_2CO_3$ solutions (pH 9.5) at 75°C and different potentials: (a) −1.0 V, (b) −0.9 V, (c) −0.6 V, (d) −0.4 V, (e) 0.0 V, (f) −0.7 V, (g) −1.0 V, and (h) −1.2 V. Curves a-e correspond to the anodic sweep, f-h to the cathodic sweep.**

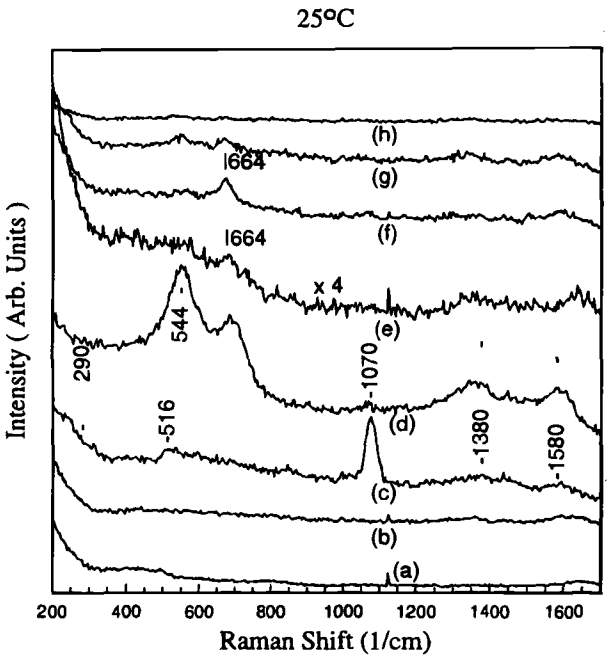


Fig. 6. SERS of iron in aerated 0.05 *M* $NaHCO_3$ + 0.001 *M* $Na_2CO_3$ solutions (pH 8.7) at 25°C and different potentials: (a) −1.0 V, (b) −0.9 V, (c) −0.6 V, (d) −0.4 V, (e) 0.0 V, (f) −0.7 V, (g) −1.0 V, and (h) −1.2 V. Curves a-e correspond to the anodic sweep, f-h to the cathodic sweep.

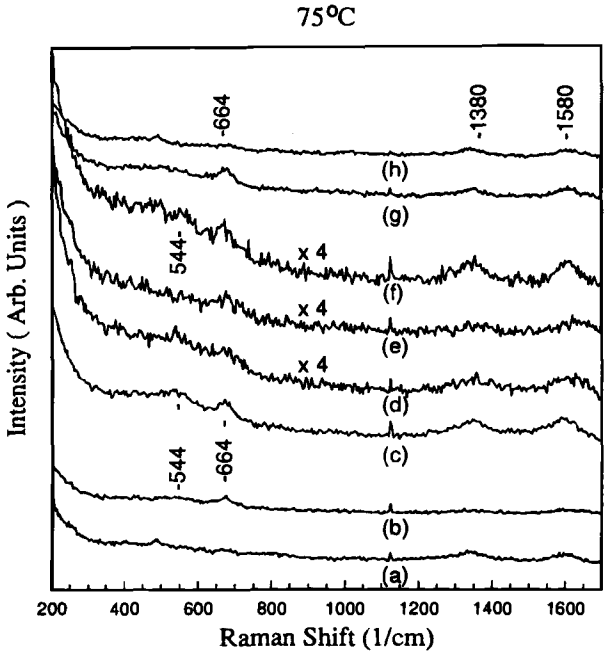


Fig. 8. SERS of iron in aerated 0.05 *M* $NaHCO_3$ + 0.001 *M* $Na_2CO_3$ solutions (pH 8.7) at 75°C and different potentials: (a) −1.0 V, (b) −0.9 V, (c) −0.6 V, (d) −0.4 V, (e) 0.0 V, (f) −0.7 V, (g) −1.0 V, and (h) −1.2 V. Curves a-e correspond to the anodic sweep, f-h to the cathodic sweep.

the 544 $cm^{-1}$ peak loses intensity after the second anodic oxidation wave. The broadening may be due to the increased contribution of the Raman signal from α-FeOOH [32] that has peaks at 490 and 680 $cm^{-1}$, γ-FeOOH with a peak near 680 $cm^{-1}$, δ-FeOOH with an even weaker Raman peak at 663 $cm^{-1}$ (that is supposed to be present during the first few oxidation-reduction cycles of the corrosion film on iron),[25] amorphous FeOOH with a peak at 700 $cm^{-1}$, [30] γ-$Fe_2O_3$ with peaks at 505 and 650 $cm^{-1}$, and perhaps an increased disorder in the oxide film.[18] Raman contributions from α-FeOOH and γ-FeOOH would be relatively weak, resulting in relatively poor spectra of these peaks. The decrease of the 544 $cm^{-1}$ intensity also indicates a decrease of $Fe(OH)_2$ in the iron corrosion film at the surface after the third anodic wave. This is expected as the dominant form of iron changes from Fe(II) to Fe(III) at these potentials. From the data given in Fig. 3 to 8e, it is not possible to determine which iron oxides or oxyhydroxides are present in the corrosion film on iron, since all of those mentioned have peaks between 500 and 700 $cm^{-1}$. The FeOOH species are expected to be present at these potentials, but the corresponding Raman signals are either small, due to the thinness of the film, or very similar to the Raman spectra from $Fe(OH)_2$ and $Fe_3O_4$. [18] An inner layer

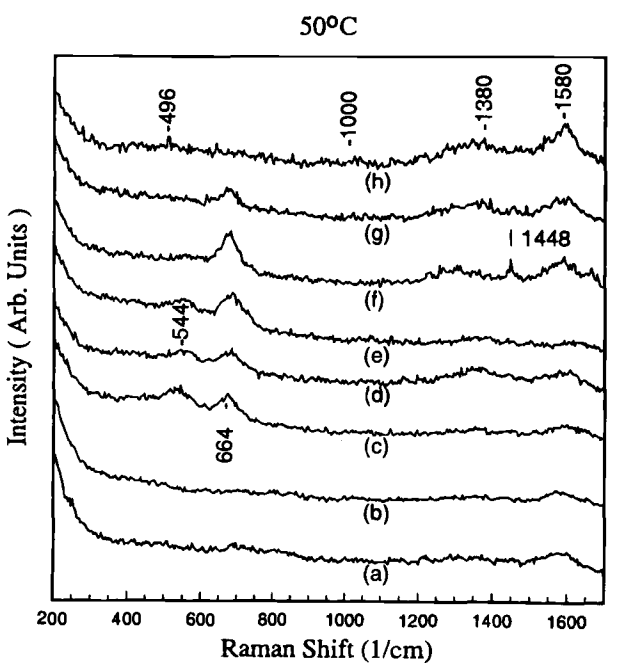


Fig. 7. SERS of iron in aerated 0.05 *M* $NaHCO_3$ + 0.001 *M* $Na_2CO_3$ solutions (pH 8.7) at 50°C and different potentials: (a) −1.0 V, (b) −0.9 V, (c) −0.6 V, (d) −0.4 V, (e) 0.0 V, (f) −0.7 V, (g) −1.0 V, and (h) −1.2 V. Curves a-e correspond to the anodic sweep, f-h to the cathodic sweep.

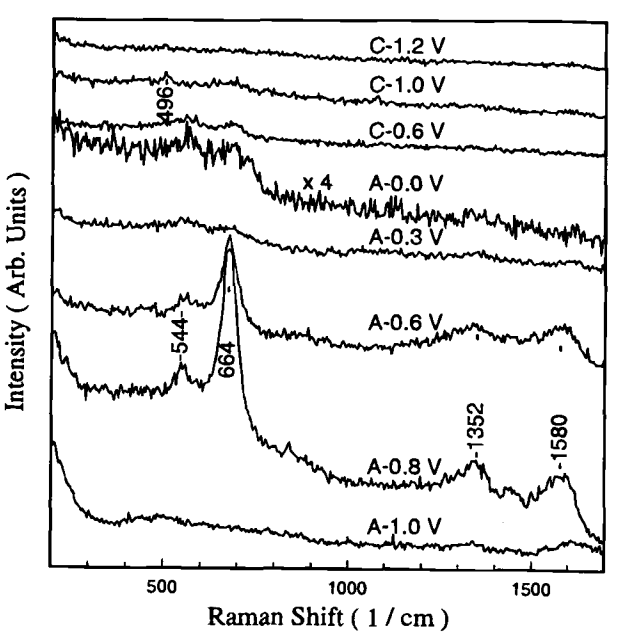


Fig. 9. SERS of iron in an aerated 0.05 *M* $Na_2CO_3$ solution (pH 11.5, 25°C) at different potentials.

of species containing $Fe^{2+}$ next to the metal surface is required by thermodynamics such that $Fe_3O_4$ may also contribute to the Raman spectrum at the higher potentials. The most appropriate conclusion is that the broadness of the peaks indicates a very disordered corrosion layer that contributes to the poor signal-to-noise ratio, and that may explain the lack of observed lattice vibrational modes between 200 and 600 $cm^{-1}$. [32] Therefore, while we expect Fe(III) species to be present in the corrosion film at 0 V (Fig. 3 to 8e) and we do observe magnetite under these conditions, any FeOOH or $Fe_2O_3$ species present must be in a relatively low density, amorphous or disordered structure, such that the Raman does not provide clear identification.

The Raman spectra after the first cathodic reduction wave (Fig. 3 to 8f) indicate an increase of $Fe(OH)_2$ and $Fe_3O_4$ at the surface. However, the 544 $cm^{-1}$ peak of $Fe(OH)_2$ is missing from the cathodic spectra at more negative potentials, indicating $Fe(OH)_2$ is reduced at potentials negative of −1.0 V. In Fig. 3 to 8, g and h, some of the spectra contain peaks at 496, 680, and 1000 $cm^{-1}$. Melendres and co-workers[21] concluded that peaks at 420, 496, 680, and 1000 $cm^{-1}$ indicated the presence of α-FeOOH in the corrosion film on iron. Kanno and Hiraiski[36] identified a Raman peak at 506 $cm^{-1}$ as an $Fe^{3+}$-$OH_2$ stretching vibration from a glassy nitrate solution. Oblonsky and Devine[18] assigned a 490 $cm^{-1}$ mode to $Fe[(H_2O)_6]^{3+}$ ions but failed to observe Raman peaks at 325 and 450 $cm^{-1}$ that are also associated with this ion.[36] The only known element that could be contributing Raman peaks at both 496 and 1000 $cm^{-1}$ in this system is α-FeOOH.[18] The obvious lack of the characteristic 390 $cm^{-1}$ Raman mode usually associated with α-FeOOH may be explained by the possible difference between an FeOOH species in the thin corrosion film and bulk crystalline FeOOH. Nauer *et al.*[32] tentatively assigned the 390 $cm^{-1}$ mode to an Fe-O stretch molecular vibration but provided very little evidence for that assignment. If the 390 $cm^{-1}$ Raman peak were a lattice mode, then the disordered nature of the corrosion film on iron and perhaps the optical parameters associated with the SERS process itself[26] would account for the lack of an observed peak at 390 $cm^{-1}$. This, along with the observations made by Tschinkel *et al.*[33] using infrared (IR) spectroscopy involving the irreversible formation of α-FeOOH on an iron electrode, would justify the tentative assignment of the 496 and 1000 $cm^{-1}$ Raman peaks to an α-FeOOH-like species in the thin corrosion film on the iron surface.[21] For this to be possible, α-FeOOH would have to be created at higher anodic potentials on some of the iron surface, but the more amorphous or disordered Fe(III) species that may have been present in the corrosion film must have masked the α-FeOOH Raman signal until most of these species were reduced at lower cathodic potentials. At 25°C, $Fe_3O_4$ and α-FeOOH are still present at least on some of the surface at the most cathodic potentials we could achieve, without the evolution of hydrogen (Fig. 3h). As demonstrated by Tschinkel *et al.*, this is attributed to the inability to reduce certain iron oxides once they have formed.[21,33] However, at 75°C the Raman peaks at −1.2 V are barely observable, qualitatively suggesting that the iron corrosion products are more easily reduced at higher temperatures.

Figure 9 illustrates the potential dependence of the Raman spectra of iron in 0.05 *M* $Na_2CO_3$ at a pH of 11.5. The results are similar to that at pH 9.5 with no siderite formation. The magnetite peak at 664 $cm^{-1}$ is larger in the divalent iron region than the 544 $cm^{-1}$ $Fe(OH)_2$ peak. This indicates that the transition from divalent to trivalent iron containing species occurs at a lower potential with increase in pH. The enhanced transition of Fe(II) to Fe(III) species at pH 11.5 may aid the formation of the passive film, and that may be associated with the observed decrease in corrosion rate at high pH.[1-6]

So far we have discussed the formation of a protective layer only in terms of divalent and trivalent iron oxides and hydroxides. Phosphate is thought to be incorporated in the passive film.[10] Iron carbonate[4-7] and calcium carbonate[8,9] have been associated with corrosion inhibition and also have been identified as actively participating in the formation of a protective film. Tillmanns[9] believed that a protective trivalent iron oxyhydrate layer containing calcium carbonate inhibited corrosion. Subsequent research discounted calcium carbonate as an active participant in the protective passive film but used an iron carbonate model to explain the relationship between carbonate and the protective layer.[7] Sontheimer *et al.*[7] assumed that a solid layer of iron carbonate acted as a transformation agent to the final iron oxyhydrate protective layer. This would predict that iron carbonate formed from divalent iron hydroxide and actively participated in the corrosion film formation. If this were true, iron carbonate should be observed in the passive film. In contrast, iron carbonate is believed by some researchers to form only in oxygen-free water and thus should not exist in the oxygenated water being investigated here.[4] This hypothesis, along with the fact that trivalent iron carbonate does not exist under these conditions, implies that one should not find any carbonate in the passive film. A recent paper by Castro *et al.*[34] described electrochemical and x-ray photoemission spectroscopy (XPS) evidence indicating carbonate was present in the iron corrosion film. However, electrochemistry is not particularly specific as to molecular composition, and XPS requires *ex situ* measurements, which may significantly alter the corrosion film from the aqueous environment. Spectroscopic studies like Raman and IR give *in situ* information about the molecular species on the electrode surface. Rubim and Dunnwald[10] obtained Raman spectra which indicated the presence of iron carbonate in the corrosion film. However, their results must be viewed critically due to the high carbonate/bicarbonate concentration used.

The Raman spectrum of Fig. 3 to 10b demonstrates that $FeCO_3$ contributes to the iron corrosion film, with oxygen present, under a very limited set of conditions (specifically, at pH < 9.5 for potentials between −0.7 and −0.5 V, and for temperatures below 50°C). The potential dependence is consistent with the Pourbaix diagram,[22] but the pH and temperature dependences observed here are more restrictive. The Raman spectra at pH ≥ 9.5 and for temperatures above 50°C have no carbonate or bicarbonate bands, indicating that no iron carbonate is present in the surface film. This directly contradicts the observations of Castro *et al.*[34] and the Raman data of Rubim and Dunnwald.[10] However, the relatively high concentrations of carbonate and bicarbonate used in those experiments and the strong pH dependence of $FeCO_3$ formation could have adversely affected their experimental results, leading to a different conclusion. Rubim and Dunnwald based their conclusion that $FeCO_3$ formed at the iron surface on the agreement of the four peaks at 290, 520 734, and 1080 $cm^{-1}$ with the standard Raman spectrum of $FeCO_3$ published by Herman *et al.*[35] However, only the small Raman peak at 509 $cm^{-1}$ is unique to $FeCO_3$. The other three peaks are due to the carbonate ion. Furthermore, Rubim and Dunnwald were not able to adequately obtain a Raman spectrum at a given potential that contained all four Raman peaks characteristic of $FeCO_3$, and still observed a 1070 $cm^{-1}$ peak above 0 V, which is past the potentials where divalent iron or iron carbonate exist. The Raman data that we collected using similar carbonate/bicarbonate concentrations to Rubim and Dunnwald indicated that the extraneous peaks at these wave numbers are mainly associated with Raman scattering from ions and soluble corrosion species in solution.

Figure 10 shows Raman spectra obtained using a 0.05 *M* $NaHCO_3$ + 0.001 *M* $Na_2CO_3$ solution at pH 8.7 and 25°C. The low carbonate concentrations in the solution do not contribute to the Raman spectra (Fig. 10a). At −0.6 V the Raman spectrum (Fig. 10b) contains peaks at 516 and 1070 $cm^{-1}$, which correspond to $FeCO_3$. [35] The Raman spectra were difficult to obtain under these conditions due to excessive generation of soluble corrosion products and particulates, which scattered the laser and Raman light and yellowed the solution. The $FeCO_3$ Raman peaks decrease as the potential

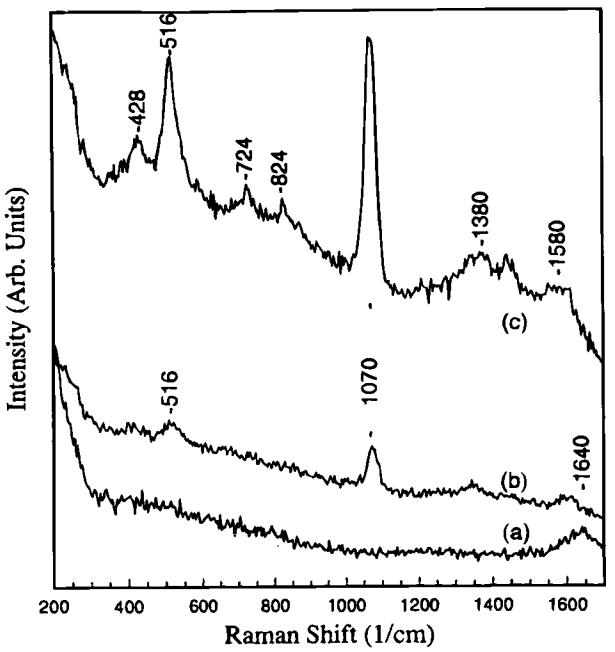


**Fig. 10. (a) Raman spectra of aqueous 0.05 *M* $NaHCO_3$ + 0.001 *M* $Na_2CO_3$ solution only (pH 8.7) at 25°C. SERS of iron in 0.05 *M* $NaCHO_3$ + 0.001 *M* $Na_2CO_3$ solutions (pH 8.7) at 25°C, (b) in aerated solution held at −0.6 V, and (c) in deaerated solution held at −0.6 V. Raman peaks at 290, 516, 724, and 1070 $cm^{-1}$ are consistent with Raman spectra from iron carbonate (siderite).**

is made more positive and vanish at −0.4 V (Fig. 6). The hypothesis that $FeCO_3$ only forms in oxygen-free environments[10] is contradicted by our results. A very strong $FeCO_3$ Raman signal is observed from the iron corrosion film at −0.6 V in deaerated solution and 25°C (Fig. 10c). The enhanced signal with peaks at 516, 724, and 1070 $cm^{-1}$ may be partly due to the increased amount of $FeCO_3$ formed on the surface and a decrease in the amount of soluble species or particulates formed in the deaerated environment. Again, identification of siderite at the interface relies mainly on the 516 $cm^{-1}$ peak that is uniquely associated with siderite when the 1070 $cm^{-1}$ carbonate peak is present. This along with the observed potential-dependent behavior of siderite and the lack of carbonate peaks under other conditions indicate that the carbonate/bicarbonate is not interacting with other components in the system.

The experiments performed here indicate that carbonate is not a component in the surface film at pH ≥ 9.5. $FeCO_3$ only forms in the corrosion film in carbonate solutions, at pH < 9.5, in a limited potential range between −0.7 and −0.5 V and for temperatures less than 50°C. $Fe(OH)_2$ and $Fe_3O_4$ are not observed while $FeCO_3$ is present in the surface film. Figure 6 indicates that $FeCO_3$ forms at a more negative potential than $Fe(OH)_2$ and $Fe_3O_4$. Therefore, $FeCO_3$ is a precursor to divalent $Fe(OH)_2$ and $Fe_3O_4$ formation. We may conclude from this, along with the limited conditions under which $FeCO_3$ forms, that $Fe(OH)_2$ is the primary intermediate species for transitions from divalent to trivalent iron,[22] and that $FeCO_3$ cannot be used as a necessary component in passivation models. The enhanced formation of soluble corrosion species while $FeCO_3$ is present in the surface film indicates that $FeCO_3$ does not inhibit iron corrosion and may aid in the chemical processes associated with corrosion. Furthermore, the lack of direct interaction of the carbonate and bicarbonate with the corrosion film suggests that the observed decrease of iron corrosion in carbonate-containing solutions is mainly due to effects of alkalinity and/or an increased buffering capacity at the iron/solution interface.

## Conclusion

The results of *in situ* SERS measurements in carbonate/bicarbonate solutions indicate that $Fe(OH)_2$ and $Fe_3O_4$ make up the majority of the prepassivation film on iron. Amorphous Fe(III) species are formed during the third anodic oxidation wave in the passive region. An α-FeOOH-like species is irreversibly formed in the iron corrosion film but is more completely reduced at temperatures above 25°C. With an increase in temperature or an increase in the solution concentration, the anodic and cathodic waves of the voltammograms become better defined. As the carbonate/bicarbonate concentration decreases, continuous anodic dissolution occurs at a lower temperature.

$FeCO_3$ formed in the corrosion film at pH < 9.5, for temperatures below 50°C, and in the potential range between −0.7 and −0.5 V (Fig. 6b, 10b, and 10c). Oxygen-free solutions increase siderite formation. Carbonate/bicarbonate does not actively participate in the formation of the corrosion film on iron for pH ≥ 9.5 or at temperatures at or above 50°C. Thus, $Fe(OH)_2$ and not $FeCO_3$ is the transformation agent to trivalent iron corrosion species. The contradictions among previously published experimental results may be explained by the limited environment that does support $FeCO_3$ formation[10,21,34] and the failure by others to distinguish between solution and surface species.

## Acknowledgment

This work was supported by the U.S. Department of Energy, Office of Energy Research, Laboratory Technology Transfer Programs, as part of a CRADA between NALCO Chemical Company and Argonne National Laboratory under Contract W-31-109-ENG-38. Valuable discussions with Dr. D. A. Johnson of NALCO are much appreciated.

Manuscript submitted June 12, 1995; revised manuscript received March 22, 1996.

*Argonne National Laboratory assisted in meeting the publication costs of this article.*

REFERENCES

1. H. H. Uhlig and R. W. Revie, *Corrosion and Corrosion Control*, John Wiley & Sons, New York (1985).
2. K. Barton, *Schutz gegen Atmospharische Korrosion*, Verlag Chemie, Weinhiem, Germany (1973).
3. H. Kaesche, *Die Korrosion der Metalle*, Springer-Verlag, New York (1986).
4. G. Bohnsack, D. A. Johnson, and E. Buss, *Proceedings of Corrosion/90*, Paper No. 438, NACE, Houston, TX (1990).
5. G. Bohnsack, D. A. Johnson, and E. Buss, *ibid.*, Paper No. 101 (1990).
6. E. Buss, I. S. DiSimone, W. S. Chiesa, G. Gasmano, G. Montesperelli, and E. Traversa, *7th SEIC Proceedings*, Vol. 9, p. 645 (1990).
7. H. Sontheimer, W. Koelle, and R. Rudek, *Korrosionsschutzschichter auf Metall von Wasser*, **52**, 1 (1979).
8. W. Stumm, *Ind. Eng. Chem.*, **51**, 12, 1487 (1959).
9. J. Tillmanns, *Gau. Wasserfach.*, **35**, 12, 845 (1927).
10. J. C. Rubim and J. Dunnwald, *J. Electroanal. Chem.*, **258**, 327 (1989).
11. M. Odziemkowski, J. Flis, and D. E. Irish, *Electrochim. Acta*, **39**, 2225 (1994).
12. C. R. Valentini, C. A. Moina, J. R. Vilche, and A. J. Arvia, *Corros. Sci.*, **25**, 985 (1985).
13. M. R. Mahoney, M. W. Howard, and R. P. Cooney, *Chem. Phys. Lett.*, **71**, 59 (1980).
14. R. P. Cooney, M. R. Mahoney, and M. W. Howard, *ibid.*, **76**, 448 (1980); R. P. Cooney, M. W. Howard, M. R. Mahoney, and T. P. Mernagh, *ibid.*, **79**, 459 (1981).
15. R. P. Frankenthal, *Electrochim. Acta*, **16**, 1845 (1971).
16. J. Kruger and J. P. Calvert, *This Journal*, **114**, 43 (1967).
17. J. Gui and T. M. Devine, *Corros. Sci.*, **32**, 1105 (1991).
18. L. J. Oblonsky and T. M. Devine, *ibid.*, **37**, 17 (1995).
19. J. Gui and T. M. Devine, *This Journal*, **138**, 1376 (1991).
20. L. J. Oblonsky, G. R. Chesnut, and T. M. Devine, Abstract 62, p. 95, The Electrochemical Society

Meeting Abstracts, Vol. 95-1, Reno, NV, May 21-26, 1995.
21. C. A. Melendres, N. Camillone III, and T. Tipton, *Electrochim. Acta*, **34**, 281 (1989); C. A. Melendres, M. Pankuch, Y. S. Li, and R. L. Kight, *ibid.*, **37**, 2747 (1992).
22. D. A. Johnson, S-H. Shim, R. V. Davis, L. J. Simpson, and C. A. Melendres, *Proceedings of the 8th European Symposium on Corrosion Inhibitors*, Ferrara, Italy (1995).
23. L. J. Simpson and C. A. Melendres, Abstract 48, p. 76, The Electrochemical Society Meeting Abstracts, Vol. 95-1, Reno, NV, May 21-26, 1995.
24. A. J. McQuillan, P. J. Hendra, and M. Fleischmann, *J. Electroanal. Chem.*, **65**, 933 (1975).
25. Y. Sasaki, N. Iwasaki, and Y. Nishina, *Surf. Sci.*, **198**, 541 (1988).
26. Y. Feng-Qi, Z. Chun-Ping, and Z. Guang-Yin, *Appl. Spectrosc.*, **43**, 1490 (1989).
27. L. Zang, C. Liu, and X. Ren, *J. Photochem. Photobiol. A*, **74**, 267 (1993).
28. R. K. Chang, *Ber. Bunsenges. Phys. Chem.*, **91**, 296 (1987).
29. I. A. Degen and G. A. Newman, *Spectrochim. Acta*, **49A**, 859 (1993).
30. J. T. Keiser and C. W. Brown, *Corros. Sci.*, 251 (1982).
31. K. Nakamoto, *Infrared and Raman Spectra of Inorganic and Coordination Compounds*, 3rd ed., p. 119, John Wiley & Sons, New York (1976).
32. G. Nauer, P. Strecha, N. Brinda-Konopik, and G. Liptay, *J. Therm. Anal.*, 813 (1985).
33. W. Tschinkel, H. Neugebauer, and A. Neckel, *This Journal*, **137**, 1475 (1990).
34. E. B. Castro, J. R. Vilche, and A. J. Arvia, *Corros. Sci.*, **32**, 37 (1991).
35. R. G. Herman, C. E. Bogdan, A. J. Sommer, and D. R. Simpson, *Appl. Spectrosc.*, **41**, 437 (1987).
36. H. Kanno and J. Hiraiski, *J. Raman Spectrosc.*, **12**, 224 (1982).

# Electrocatalytic Properties of Co, Pt, and Pt-Co on Carbon for the Reduction of Oxygen in Alkaline Fuel Cells

**Yohannes Kiros**

*Department of Chemical Engineering and Technology, Chemical Technology, Royal Institute of Technology, S-100 44 Stockholm, Sweden*

ABSTRACT

The effect of cobalt, platinum, and cobalt-platinum, alloys on high surface area carbons for oxygen reduction in alkaline electrolyte was investigated. The Pt-Co catalyst with *ca.* 1:3 atomic ratio was prepared by addition of $H_2PtCl_6$ solution to a mixture of methanol and a 5% surfactant in deionized water containing cobalt acetate and carbon suspension. This was followed by drying and heat-treatment at 700 and 900°C in a flow of hydrogen and nitrogen gas mixtures. Polarization curves and kinetic parameters for Pt, Co, and Pt-Co were conducted and compared in 6 *M* KOH and at 80°C. Higher activities were observed for the Pt-Co alloy, that had been heat treated at 900°C. In addition to increased activity of this catalyst, the unalloyed base metal (Co) contributes to total performance improvement of the oxygen reduction process. Furthermore, surface, structural, and chemical characterizations of the catalysts were carried out using transmission electron microscopy, x-ray diffraction, Brunauer, Emmett, and Teller method, and atomic absorption spectroscopy. Dissolution of cobalt from the electrodes, both from the single cobalt phase and Pt-Co alloy catalysts, has been established. The x-ray results demonstrated a shift to lower lattice parameters (3.618 Å) by the Pt-Co alloys, prepared at 900°C, than the pure platinum catalyst (3.919 Å).

Platinum is the most widely used electrocatalyst for medium and low temperature fuel cells, *i.e.*, phosphoric acid (PAFC), polymer electrolyte (PEFC), and alkaline fuel cells (AFC). This catalyst applied on carbons, however, experiences corrosion and agglomeration.[1,2] In aqueous electrolytes, platinum is subjected to agglomeration leading to surface area loss and decreased electrode performance, which restricts long-term operation of the fuel cell. Blurton *et al.*[3] have shown that the platinum surface area loss was relatively insensitive to electrode operating potential and that crystallite migration is the dominating mechanism of supported platinum surface area loss. Tomantscheger *et al.*[4] have reported that on exposure of carbon-supported platinum catalysts to potassium hydroxide, the size of the agglomerates increased with logarithmic dependence over a period of 48 h. The platinum particle size during this time increased fourfold, *i.e.*, from less than 50 to 200 Å. Other mechanisms, such as Pt dissolution, redeposition, and dependence on electrode potentials,[5,6] surface migration and coalescence and/or diffusion of platinum atoms and crystallites[7-9] have been found to be the main causes of agglomeration. Thus, as oxygen reduction catalysis in aqueous electrolyte is a structure-sensitive reaction,[10,11] *i.e.*, the specific activity of the electrodes is related to the Pt crystallite size, surface modifications of the catalyst is a prior requirement and one of the main areas of research for circumventing problems associated with platinum or combination of it with other associated metals in fuel cells.

Binary or tertiary metals or alloy surfaces and bimetallic combinations have in the last few years gained increased attention as oxygen reduction electrocatalysts in fuel cells and/or for direct electrochemical oxidation of methanol.[12] These catalysts which are composed of Pt-M surfaces dispersed on high surface area carbon supports, where M denotes a 3d transition metal (*e.g.*, Ti, Cr, Fe, Co, Cu, etc.) have shown enhanced catalytic activities and stable chemical properties. The importance of these new catalyst systems have been shown in numerous patents and studies[13-19] describing the role of alloying platinum with transition metals. Jalan and Taylor[20] have suggested that the distance between nearest neighbor platinum atoms on the surface of a supported catalyst is not ideal for dual site adsorption of oxygen and peroxide and that introduction of foreign atoms which reduce the platinum nearest neighbor spacing results in higher oxygen reduction activity. Beard and Ross[16] as well as Paffett *et al.*[17] have suggested that surface roughness effects due to dissolution of the transition metal give a surface area effect and hence a significant enhancement of the oxygen reduction reaction. While all alloys studied in Ref. 13-20 were carried out in acid electrolytes and with Pt to transition metal ratios of 3:1, this study presents alloy compositions contrary to this ratio and gives performance characteristics in alkaline electrolyte.

Our aim here is to report a preparative method of the high surface area carbon-supported platinum, cobalt, and Pt-Co mixtures, heat-treated at high temperatures and to